Nanoscale

PAPER

View Article Online
View Journal | View Issue

Cite this: *Nanoscale*, 2024, **16**, 16451

Modulated assembly and structural diversity of heterometallic Sn–Ti oxo clusters from inorganic tin precursors†

Hui-Fang Zhao,[a] Fang-Fang Liu,[a] Qing-Rong Ding,[a] Di Wang,[a] Jian Zhang [a] and Lei Zhang *[a,b]

Received 26th June 2024,
Accepted 9th August 2024

DOI: 10.1039/d4nr02644f

rsc.li/nanoscale

Through modulating the multidentate ligands, solvent environments, and inorganic tin precursors during the synthesis processes, we have successfully prepared a series of unprecedented heterometallic Sn–Ti oxo clusters with structural diversity and different physiochemical attributes. Initially, two **Sn_6Ti_{10}** clusters were synthesized using trimethylolpropane as a structure-oriented ligand and $SnCl_4{\cdot}5H_2O$ as a tin source. Then, when a larger pentadentate ligand di(trimethylolpropane) was used instead of trimethylolpropane and aprotic acetonitrile solvent was introduced into the reaction system, four low-nuclearity Sn–Ti oxo clusters were discovered, including two **Sn_1Ti_1**, one **Sn_2Ti_2** and one **Sn_2Ti_6**. Finally, two mixed-valence state clusters, **$Sn^{II}_4Sn^{IV}_2Ti^{IV}_{14}$** and **$Sn^{II}_4Sn^{IV}_4Ti^{IV}_{20}$**, were obtained by transforming the tin precursor from $SnCl_4{\cdot}5H_2O$ to $SnCl_2{\cdot}2H_2O$ and adjusting the acetonitrile solution with trace acetic acid/formic acid. **Sn_8Ti_{20}** is the highest-nuclearity heterometallic Sn–Ti oxo cluster to date. Moreover, comparative electrocatalytic CO_2 reduction experiments were carried out, and it was concluded that the **Sn_8Ti_{20}**-decorated electrode showed the most satisfactory performance due to the influence of mixed-valence states of the Sn atoms and the charging effects provided by 20 Ti^{4+} ions. This study presents important guiding significance for the design, synthesis and application optimization of functional heterometallic nanoclusters.

Introduction

Studying the formation mechanisms, structures, and properties of clusters not only builds a bridge between atoms/molecules and condensed states of matter, but also helps us to conduct precise research on molecular materials.[1] Therefore, in recent years, the chemistry of metal oxo clusters (MOCs) has developed rapidly and MOCs with accurate atomic structural information have been synthesized continuously.[2–6] Doping heteroatoms with metal oxides is considered one of the most effective ways to improve the catalytic performance of materials.[7,8] This might occur because the composite material produces synergistic effects to improve its catalytic performance.[9,10] Similarly, heterometallic oxo clusters combine the characteristics of MOCs and the interaction between different kinds of metals in their composition, thus giving the materials unique physical and chemical properties.[11–16] However, although both homometallic Ti- and Sn-oxo clusters have been extensively reported, the number of heterometallic Sn–Ti oxo clusters is relatively small at present. Extensive research in this field has been limited to the discovery of a few Sn–Ti oxo clusters with low nuclearity (≤11), such as $\{Sn_1Ti_1\}$,[17,18] $\{Sn_1Ti_2\}$,[19,20] $\{Sn_3Ti_1\}$,[21] $\{Sn_4Ti_1\}$,[22] $\{Sn_2Ti_6\}$,[23] $\{Sn_4Ti_6\}$[24] and $\{Sn_6Ti_5\}$.[25] Very recently, we prepared three dual-layered Sn–Ti oxo clusters, two $\{Sn_2Ti_{12}\}$ and one $\{Sn_6Ti_{14}\}$, which were functionalized with 1,10-phenanthroline and showed interesting optical limiting effects.[26] Therefore, it is necessary to develop high-nuclearity Sn–Ti oxo clusters to enrich their structures and expand applications.

In the synthesis of tin oxo clusters, organotin compounds have been used as the main tin sources, while a few examples have been prepared using inorganic tin sources. There is a significant difference between organotin and inorganic tin precursors in the synthesis reactions.[27–30] Moreover, unlike the single valence state of organic tin sources, inorganic tin precursors have two different valence states: +2 and +4.[23,31,32] In addition, an important advantage of MOCs is that their modifiable surface organic ligands can regulate the structures of the obtained clusters and improve their properties.[33–35]

[a]*State Key Laboratory of Structural Chemistry, Fujian Institute of Research on the Structure of Matter, Chinese Academy of Sciences, Fuzhou, Fujian 350002, China*
[b]*Institute of Modern Optics, College of Electronic Information and Optical Engineering, Nankai University, Tianjin 300350, China.*
E-mail: zhanglei3915@nankai.edu.cn

†Electronic supplementary information (ESI) available. CCDC 2365528–2365535 (**TOC-51–TOC-58**). For ESI and crystallographic data in CIF or other electronic format see DOI: **https://doi.org/10.1039/d4nr02644f**

Compared with organotin precursors, inorganic tin precursors not only are more environmentally friendly, but also more easily break Sn–X (F, Cl, Br, I, *etc.*) bonds, which are more likely to be modified by functional organic ligands during the reaction process.[30]

Usually, the multiple coordination modes of multidentate ligands can meet the spatial requirements and stabilize MOCs to the greatest extent.[36–38] Herein, polyhydroxyalkanes with multiple mildly acidic hydroxyl groups were selected as the protecting ligands for the construction of heterometallic Sn–Ti oxo clusters, including trimethylolpropane (H_3TPP) and di(trimethylolpropane) (H_4DTPP). Through comprehensively adjusting solvents, tin precursors, temperature and other synthetic factors, the modulated assembly of a series of Sn–Ti oxo clusters was achieved (Table 1). As a result, seven intermediates were successfully identified, including two **Sn_6Ti_{10}** clusters (**TOC-51** and **TOC-52**), two **Sn_1Ti_1** clusters (**TOC-53** and **TOC-54**), one **Sn_2Ti_2** cluster (**TOC-55**), one **Sn_2Ti_6** cluster (**TOC-56**), and one **Sn_6Ti_{14}** cluster (**TOC-57**), guiding to the targeted **Sn_8Ti_{20}** cluster (**TOC-58**) eventually (Scheme 1). Among these, **TOC-57** and **TOC-58** show interesting mixed Sn^{2+}/Sn^{4+} valences which were proved by bond-valence sum (BVS) calculations (Tables S5 and S6†), X-ray photoelectron spectroscopy (XPS) analysis (Fig. 1) and the charge balancing principle. The windmill-like structure of **TOC-58** embodies a unique structural aesthetic. The core size of **TOC-58** is ~0.8 × 2.2 nm, and its nuclearity of 28 exceeds those of currently known heterometallic Sn–Ti oxo clusters (≤20). Electrocatalytic CO_2 reduction (CO_2RR) studies were conducted on three large clusters (**TOC-51**, **TOC-57** and **TOC-58**), and the experimental results showed that the formate Faradaic efficiency ($FE_{formate}$) of the electrode derived from **TOC-58** with the largest $\{Sn_8Ti_{20}\}$ core and mixed Sn^{2+}/Sn^{4+} valences reached above 66% at −1.0 (*vs.* RHE).

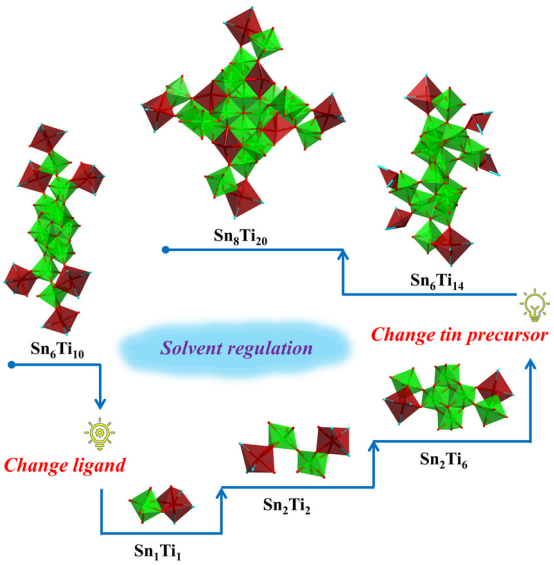

Scheme 1 Illustration of the synthetic route from intermediates (**Sn_6Ti_{10}**, **Sn_1Ti_1**, **Sn_2Ti_2**, **Sn_2Ti_6**, and **Sn_6Ti_{14}**) to the largest **Sn_8Ti_{20}**.

Results and discussion

In the initial stage of this research, using $SnCl_4{\cdot}5H_2O$, trimethylolpropane and $Ti(O^iPr)_4$ as raw materials, a colorless crystal of **TOC-51** was synthesized by allowing it to stand at room temperature for 6 days after heating at 80 °C for 3 days in a mixture of 1,4-dioxane solvent and ethyl acetate. Ethyl acetate is easily hydrolyzed and will gradually produce acetic acid and ethanol during the reaction. As shown in Fig. 2a, single-crystal X-ray diffraction analysis indicates that trimethylolpropane collaborates with the auxiliary ligand HAc to form the hamburger-like structure of **TOC-51**. The protected inorganic Sn_2Ti_8 core is linked with two $\{Sn_2Ti(TPP)(HTPP)Cl_6\}$ units by four μ_2-O to form the whole **TOC-51** cluster. The bread slices of the hamburger are $\{Sn_2Ti(TPP)(HTPP)Cl_6\}$ moieties. The Sn_2Ti_8 core in the middle of the structure is composed of two μ_4-O and two μ_3-O connecting eight Ti atoms, while two Sn atoms are bonded to the Ti atoms by μ_2-OH. In fact, there are two ways for O atoms in H_3TPP to participate in the coordination. One is that two O atoms take part in the coordination and the other is that all three O atoms take part in the coordination. The Sn_2Ti_8 core is surrounded by six trimethylolpropanes, two acetic acids, and six Cl atoms. For the two Sn atoms in Sn_2Ti_8, there are two H_2O molecules participating in their 6-coordination, respectively. Meanwhile, the acetic acid in **TOC-51** can be replaced with propionic acid to form another new cluster **TOC-52** (Fig. 2e). Although the two clusters are structurally identical except for modifying the same sites with

Table 1 Summary of the composition and reaction conditions of **TOC-51** to **TOC-58**

Compound	Ligand	Sn source	Solvent		Formula
TOC-51	H_3TPP	$SnCl_4{\cdot}5H_2O$	1,4-Dioxane	Ethyl acetate	$[Sn^{IV}_6Ti^{IV}_{10}(\mu_4\text{-O})_2(\mu_3\text{-O})_2(\mu_2\text{-O})_4(\mu_2\text{-OH})_2(TPP)_6(HTPP)_4(Ac)_2(H_2O)_2\ Cl_{18}]{\cdot}2(1,4\text{-D})$
TOC-52	H_3TPP			Propionic acid	$[Sn^{IV}_6Ti^{IV}_{10}(\mu_4\text{-O})_2(\mu_3\text{-O})_2(\mu_2\text{-O})_4(\mu_2\text{-OH})_2(TPP)_6(HTPP)_4(Pr)_2(H_2O)_2\ Cl_{18}]{\cdot}2(1,4\text{-D})$
TOC-53	H_4DTPP		Acetonitrile	Ethyl acetate	$[Sn^{IV}Ti^{IV}(DTPP)(Ac)Cl_3]$
TOC-54	H_4DTPP			Propionic acid	$[Sn^{IV}Ti^{IV}(DTPP)(Pr)Cl_3]$
TOC-55	H_4DTPP			1,4-Dioxane	$[Sn^{IV}_2Ti^{IV}_2(\mu_2\text{-O})(DTPP)_2(H_2O)_2Cl_6]$
TOC-56	H_4DTPs			Propionic acid	$H_2[Sn^{IV}_2Ti^{IV}_6(\mu_2\text{-O})_6(DTPP)_4Cl_6]$
TOC-57	H_4DTPP	$SnCl_2{\cdot}2H_2O$		Acetic acid	$[Sn^{II}_4Sn^{IV}_2Ti^{IV}_{14}(\mu_4\text{-O})_2(\mu_3\text{-O})_4(\mu_2\text{-O})_8(DTPP)_6(HDTPP)_2Cl_{14}]$
TOC-58	H_4DTPP			Formic acid	$[Sn^{II}_4Sn^{IV}_4Ti^{IV}_{20}(\mu_4\text{-O})_8(\mu_3\text{-O})_4(\mu_2\text{-O})_{10}(DTPP)_{12}Cl_{12}]$

Abbreviations: H_3TPP = trimethylolpropane; H_4DTPP = di(trimethylolpropane); HPr = propionic acid; HAc = acetic acid; 1,4-D = 1,4-dioxane.

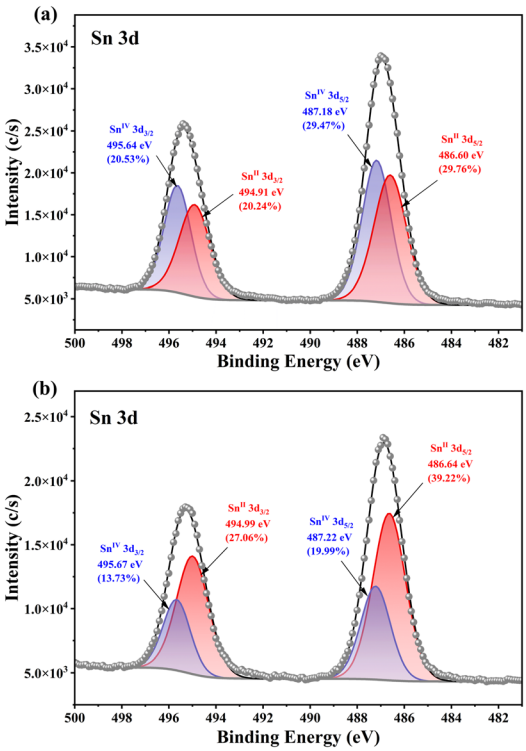

Fig. 1 XPS spectra of Sn 3d of **TOC-57** (a) and **TOC-58** (b).

different carboxylic acids, they are different in the packing modes (Fig. 2c and f). Both Sn atoms and Ti atoms exist with 6-coordination and +4 valence in the above two $\mathbf{Sn_6Ti_{10}}$ clusters (**TOC-51** and **TOC-52**).

When only replacing the small-sized tridentate ligand H_3TPP with the larger pentadentate ligand H_4DTPP, there was no crystal growth in the original solvent environment. Through debugging the solvent, it was found that when aprotic solvent CH_3CN was used, four new heterometallic Sn–Ti oxo clusters (**TOC-53–TOC-56**) were constructed with different auxiliary solvents (Fig. 3). **TOC-53** was formed by the synergistic coordination of the organic ligand H_4DTPP and the auxiliary ligand HAc from the decomposition of ethyl acetate solvent molecules. Just as the acetic acid in **TOC-51** can be substituted by propionic acid to obtain **TOC-52**, the acetic acid in **TOC-53** also can be replaced by propionic acid to give rise to **TOC-54**. The packing diagrams of **TOC-53** and **TOC-54** are also dissimilar (Fig. S1b and S2b†). **TOC-55** can be seen as the connection of two **TOC-51** clusters through a μ_2-O between two Ti atoms, relying on H_2O molecules to stabilize the 6-coordinate mode of Sn atoms. When we reduced the dosage of propionic acid to 50 μL while keeping the other conditions unchanged, **TOC-56** was found. As shown in Fig. 3, **TOC-56** can be regarded as the insertion of two DTPP ligands protecting four Ti atoms in the middle of the **TOC-55** structure. In these four Sn–Ti heterometallic oxo clusters (**TOC-53–TOC-56**), Sn atoms and Ti atoms also exist in 6-coordinated and +4 valence states. Furthermore, energy dispersive spectroscopy (EDS) and plasma emission spectroscopy (ICP) analyses matched well with the obtained crystallographic results (Fig. S12–S15 and Table S7†).

Nevertheless, the cluster nuclearity was unable to further increase through continually adjusting the dosage of propionic acid or replacing propionic acid with other stronger/weaker acids. To break this deadlock, we considered introducing an inorganic tin raw material as $SnCl_2{\cdot}2H_2O$ with better reactivity. Fortunately, **TOC-57** with a larger Sn_6Ti_{14} core was obtained by changing the tin source from $SnCl_4{\cdot}5H_2O$ to $SnCl_2{\cdot}2H_2O$ and adjusting the acetonitrile solution with trace acetic acid (Fig. 4a). The cluster structure of **TOC-57** can be seen to trans-

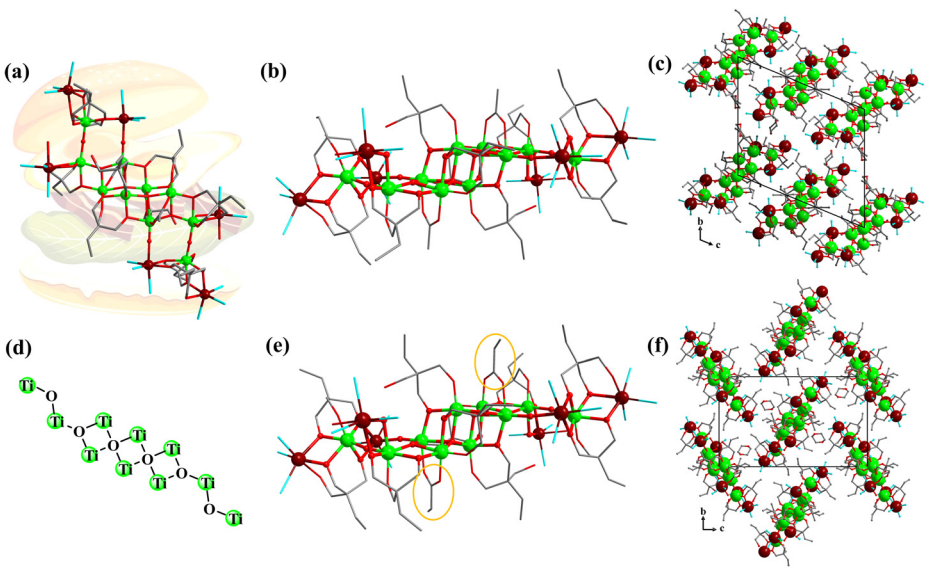

Fig. 2 (a and b) Hamburger-like structure of **TOC-51**. (c) Packing mode of **TOC-51**. (d) Connection diagram of Ti atoms through bridging an O atom in **TOC-51**. (e) Cluster structure of **TOC-52**, highlighting the Pr ligands. (f) Packing mode of **TOC-52**. Color codes: dark red, Sn; green, Ti; blue, Cl; gray, C; red, O. H atoms were omitted for clarity.

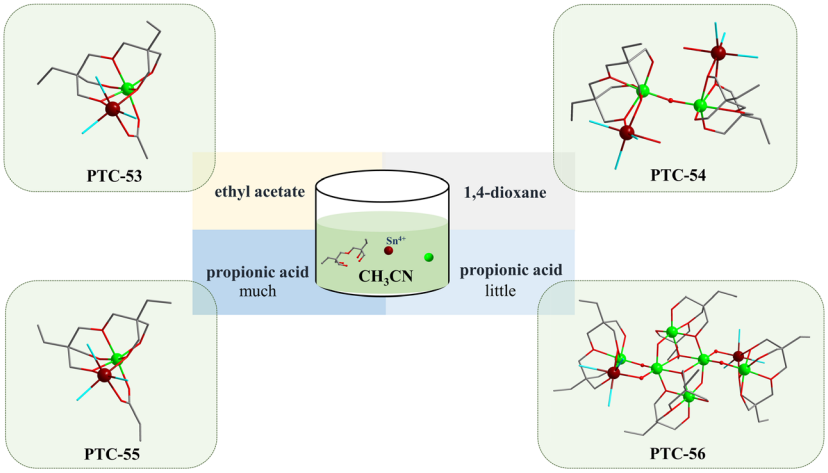

Fig. 3 Synthetic conditions and cluster structures of **TOC-53–TOC-56**.

form the four Ti atoms protected by DTPP ligands in the middle of **TOC-56** into a Sn_4Ti_{12} inorganic core encircled by DTPP ligands, to achieve a further increase in the number of cluster cores. Interestingly, BVS calculations (Table S5†) and XPS analysis (Fig. 1a) showed that the tin ions in **TOC-57** were in mixed-valence states due to the partial oxidation of the initial Sn^{2+} ions during the synthesis process. The four Sn atoms in the Sn_4Ti_{12} inorganic core display 3-coordination and +2 valence states. Therein, two Sn^{2+} ions are bridged with Ti atoms by two O atoms from two DTPP ligands and the other two Sn^{2+} ions are linked with Ti atoms by a μ_2-O. The 12 Ti atoms in the inorganic core Sn_4Ti_{12} are connected together by 4 μ_2-O, 2 μ_3-O, and 2 μ_4-O. There are 6- and 7-coordination modes for Ti atoms, with two out of 14 Ti atoms being 7-coordinated.

Based on the above synthesis results, we can clearly see that the assembly of heterometallic Sn–Ti oxo clusters was greatly affected by solvents and the pH value of the solution also played an important role in the assembly of the cluster core in this system. Accordingly, when we further replaced acetic acid with more acidic formic acid and the other conditions remained unchanged from those for **TOC-57**, a highly symmetric high-nuclearity Sn–Ti oxo cluster **TOC-58** was synthesized (Fig. 5b). The cluster core of **TOC-58** is Sn_8Ti_{20}, which represents the nuclearity record in the existing heterometallic Sn–Ti oxo clusters. The results of single-crystal X-ray diffraction show that it crystallizes in a cubic system with the space group $I\bar{4}3d$. The atomic ratio of Sn to Ti was determined to be 8 : 20.09 through ICP analysis (Table S7†), which is consistent with the structural analysis results. The cluster core size of

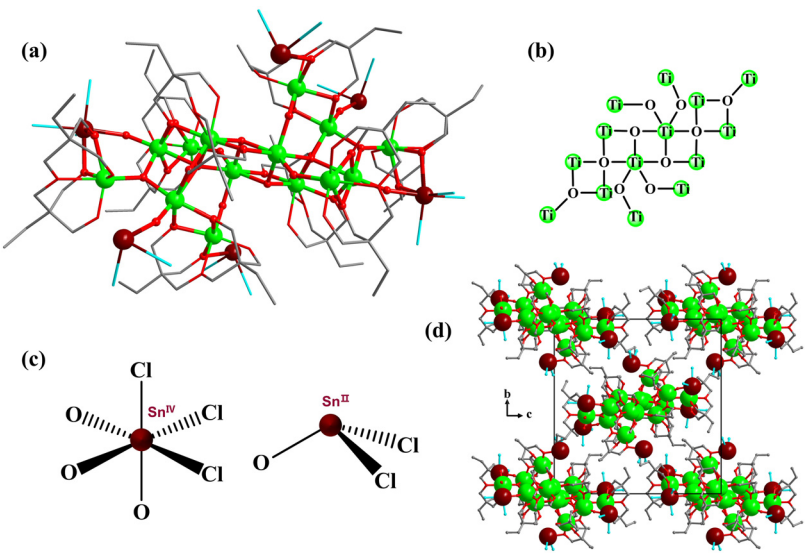

Fig. 4 (a) The cluster structure of **TOC-57**. (b) Connection diagram of Ti atoms through bridging an O atom in **TOC-57**. (c) Coordination spheres of the Sn atoms in **TOC-57**. (d) The packing mode of **TOC-57**.

TOC-58 is ~2.2 × 0.8 nm (Fig. 5e). The crystal structure analysis reveals that **TOC-58** has a central scale structure, and the whole cluster is like a windmill. At the top of the four blades of the windmill there are {SnTi(DTPP)Cl_3} units, and the internal inorganic core is Sn_4Ti_{16} (Fig. 5a). The Sn_4Ti_{16} inorganic core of **TOC-58** consists of four μ_4-O bridged {$SnTi_3$} tetranuclear parts and four Ti atoms are connected by four μ_2-O. The two adjacent {$SnTi_3$} tetranuclear moieties are connected by a μ_4-O, and the linker between two opposite {$SnTi_3$} tetranuclear parts is one μ_2-O bridge. Moreover, each of the four Ti atoms forming the central scale has a μ_2-O attached to a Ti atom. Four Ti atoms and four {$SnTi_3$} tetranuclear moieties are distributed before and after in a regular pattern. The Sn_4Ti_{16} inorganic core is surrounded by eight DTPP ligands. The tin atoms in **TOC-58** are also in mixed-valence states as proved by BVS calculations (Table S6†) and XPS analysis (Fig. 1b). Different from the 3-coordination mode of Sn^{2+} ions in **TOC-57** (Fig. 4c), the Sn^{2+} ions in **TOC-58** adopt the 5-coordination mode (Fig. 5c). The 5-coordination tin atoms are connected to the 7-coordination Ti atoms by a μ_4-O. In addition, the Ti^{4+} ions in **TOC-58** are located in the {TiO_7} or {TiO_6} coordination geometry. Among the 20 Ti atoms, four are 7-coordinated which are distributed in four cubes, respectively. Because inorganic tin precursors are used, the Sn^{4+} ions in all clusters (**TOC-51–TOC-58**) are located in the {SnO_3Cl_3} coordination octahedra. By analysing the TG curve of **TOC-58** (Fig. S19d†), it was observed that the skeleton of the compound remained relatively stable until ~300 °C. Beyond this temperature, ligand detachment and structural decomposition occurred.

Sn containing materials are regarded as suitable CO_2RR electrocatalysts to produce formic acid.[39–46] Considering that **TOC-51**, **TOC-57** and **TOC-58** present potential active sites of Sn atoms (Fig. S7†), their applications in electrocatalysis were studied. First, linear sweep voltammetry (LSV) profiles of the three sample-modified working electrodes were measured in 0.5 M $KHCO_3$ solution filled with N_2 or CO_2 (Fig. 6a). It was clear that the current densities of **TOC-51**-, **TOC-57**- and **TOC-58**-derived electrodes in CO_2-saturated electrolyte were higher than those in N_2-saturated electrolyte, revealing the capacity of the CO_2RR. The **TOC-58**-modified electrode displayed the lowest initial potential, indicating the fastest electrocatalytic kinetics. The liquid product of the CO_2RR was detected by nuclear magnetic resonance spectroscopy (Fig. S25†), and the analysis demonstrated that formate was the only liquid product. The FE_{formic} was measured by ion chromatography (Fig. S26†), and the values for H_2 (Fig. S27†) and CO (Fig. S28†) were measured by gas chromatography.

As shown in Fig. 6b, the $FE_{formate}$ of the **TOC-51**-modified electrode shows little difference under different voltages with the highest value being ~51% at −1.0 V (*vs.* RHE). The electrode modified with **TOC-57** exhibits the lowest $FE_{formate}$ at −0.7 (*vs* RHE) and it increases to around 57% at −1.0 V (*vs.* RHE). The highest $FE_{formate}$ of the electrode modified with **TOC-58** exceeds 66% at −1.0 (*vs.* RHE). Although the number of Sn active sites in **TOC-58** is less than that in **TOC-57**, it contains more Ti^{4+} to achieve better charging effects.[24] Meanwhile, the mixed-valence states of Sn atoms show better catalytic activity than the single valence state.[31] These compre-

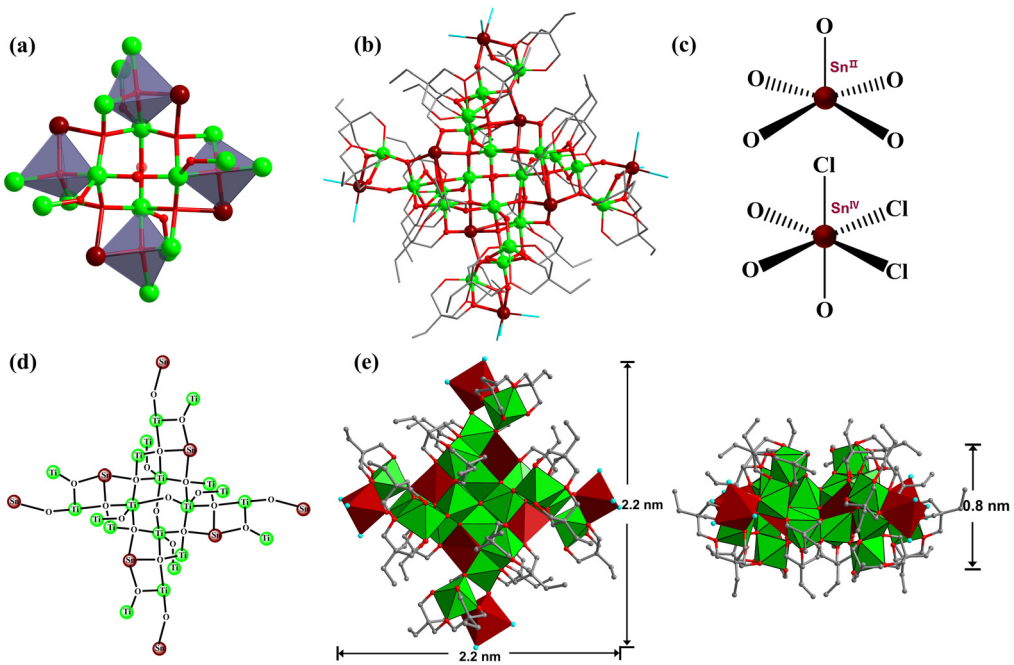

Fig. 5 (a) Multifaceted view of the Sn_4Ti_{16} internal inorganic core in **TOC-58**. (b) The cluster structure of **TOC-58**. (c) Coordination spheres of the Sn atoms in **TOC-58**. (d) Connection diagram of Ti and Sn atoms through bridging an O atom in **TOC-58**. (e) Polyhedral representations of the Sn_8Ti_{20} core of **TOC-58**.

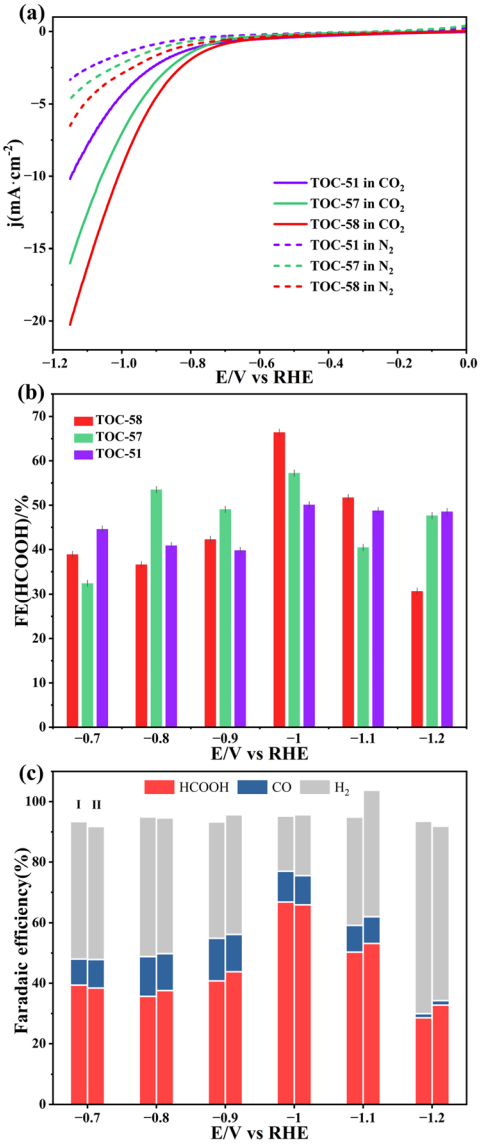

Fig. 6 (a) LSV profiles of **TOC-51**-, **TOC-57**- and **TOC-58**-decorated electrodes in N_2-or CO_2-saturated 0.5 M $KHCO_3$ solution. (b) Comparative FEs of formates for **TOC-51**-, **TOC-57**- and **TOC-58**-derived electrodes at various potentials. (c) Faradaic efficiencies for formats H_2 and CO at different potentials of the **TOC-58**-decorated electrode, showing the results of two different experiments (I and II).

hensive factors make **TOC-58** exhibit the best catalytic effect. The stability of these cluster decorated electrodes was confirmed by the well-maintained mass spectrometry and XPS spectra after electrocatalysis (Fig. S31–S33†).

Conclusions

In conclusion, we used inorganic tin precursors and functional tridentate H_3DPP and pentadentate H_4DTPP ligands to direct the assembly of heterometallic Sn–Ti oxo clusters. A family of compounds with various nuclearities was successfully constructed by adjusting the solvents and changing the inorganic tin sources. Therein, $\mathbf{Sn_8Ti_{20}}$ (**TOC-58**) presents the highest nuclearity and the largest size in the heterometallic Sn–Ti oxo cluster field. Moreover, mixed Sn^{2+}/Sn^{4+} valent states have been achieved by the introduction of $SnCl_2{\cdot}2H_2O$ during synthesis. Both the mixed-valence states of Sn atoms and the charging effects of Ti^{4+} ions show influence on the electrocatalytic activity of these heterometallic Sn–Ti oxo clusters, with the **TOC-58**-decorated electrode exhibiting the highest $FE_{formate}$ (over 66%). This work not only enriches the structural diversity of Sn–Ti oxo clusters, but also provides an efficient strategy for improving their physiochemical performance.

Data availability

The data supporting this article have been included as part of the ESI.†

Crystallographic data for **TOC-51** to **TOC-58** have been deposited at the Cambridge Crystallographic Data Centre (CCDC) deposition numbers 2365528 to 2365535.

Conflicts of interest

There are no conflicts to declare.

Acknowledgements

This work was supported by the Natural Science Foundation of Fujian Province (2022J02013) and the National Natural Science Foundation of China (22271284).

References

1 L. Liu and A. Corma, *Chem. Rev.*, 2018, **118**, 4981–5079.
2 J. C. Liu, J. F. Wang, Q. Han, P. Shangguan, L. L. Liu, L. J. Chen, J. W. Zhao, C. Streb and Y. F. Song, *Angew. Chem., Int. Ed.*, 2021, **60**, 11153–11157.
3 N. I. Gumerova and A. Rompel, *Chem. Soc. Rev.*, 2020, **49**, 7568–7601.
4 X. Y. Zheng, Y. H. Jiang, G. L. Zhuang, D. P. Liu, H. G. Liao, X. J. Kong, L. S. Long and L. S. Zheng, *J. Am. Chem. Soc.*, 2017, **139**, 18178–18181.
5 D. Wang, X. F. Yi and L. Zhang, *Sci. China: Chem.*, 2021, **65**, 114–119.
6 P. Yang and U. Kortz, *Acc. Chem. Res.*, 2018, **51**, 1599–1608.
7 L. Yang, J. Lei, J. M. Fan, R. M. Yuan, M. S. Zheng, J. J. Chen and Q. F. Dong, *Adv. Mater.*, 2021, **33**, e2005019.
8 X. Yang, D. Schipper, R. A. Jones, L. A. Lytwak, B. J. Holliday and S. Huang, *J. Am. Chem. Soc.*, 2013, **135**, 8468–8471.
9 G. Soldan, M. A. Aljuhani, M. S. Bootharaju, L. G. AbdulHalim, M. R. Parida, A. H. Emwas,

O. F. Mohammed and O. M. Bakr, *Angew. Chem., Int. Ed.*, 2016, **55**, 5749–5753.
10 H. Zhang, M. Jin and Y. Xia, *Chem. Soc. Rev.*, 2012, **41**, 8035–8049.
11 F. F. Liu, D. Wang, G. H. Chen, Y. Qiao, F. Luo, J. Zhang and L. Zhang, *Sci. China: Chem.*, 2023, **66**, 1731–1736.
12 J. X. Liu, X. B. Zhang, Y. L. Li, S. L. Huang and G. Y. Yang, *Coord. Chem. Rev.*, 2020, **414**, 213260.
13 Y. Liu, Y. Li, Y. Yang, J. Zhu and K. Wu, *Sci. China: Chem.*, 2023, **66**, 3628–3635.
14 B. L. Han, Z. Wang, R. K. Gupta, L. Feng, S. Wang, M. Kurmoo, Z. Y. Gao, S. Schein, C. H. Tung and D. Sun, *ACS Nano*, 2021, **15**, 8733–8741.
15 Z. Wang, R. Senanayake, C. M. Aikens, W. M. Chen, C. H. Tung and D. Sun, *Nanoscale*, 2016, **8**, 18905–18911.
16 G. Zhang, M. Baranov, F. Wang, J. M. Poblet, S. Kozuch, N. Leffler, A. I. Shames, J. M. Clemente-Juan, A. Neyman and I. A. Weinstock, *J. Am. Chem. Soc.*, 2021, **143**, 20769–20778.
17 S. Mishra, E. Jeanneau, S. Mangematin, H. Chermette, M. Poor Kalhor, G. Bonnefont, G. Fantozzi, S. Le Floch, S. Pailhes and S. Daniele, *Dalton Trans.*, 2015, **44**, 6848–6862.
18 S. Mishra, E. Jeanneau, L. Tian, I. Nuta, E. Blanquet, D. Singh, R. Ahuja, C. Marichy and S. Daniele, *Cryst. Growth Des.*, 2021, **22**, 54–59.
19 M. Veith, S. Mathur, C. Mathur and V. Huch, *Organometallics*, 1998, **17**, 1044–1051.
20 S. Mishra, E. Jeanneau, M. H. Berger, J. F. Hochepied and S. Daniele, *Inorg. Chem.*, 2010, **49**, 11184–11189.
21 T. J. Boyle, J. M. Segall, T. M. Alam, M. A. Rodriguez and J. M. Santana, *J. Am. Chem. Soc.*, 2002, **124**, 6904–6913.
22 Q. Zhang, H. D. Lai and Q. P. Lin, *J. Solid State Chem.*, 2021, **297**, 122056.
23 D. Wang, G. H. Chen, L. B. Yuan, C. C. Feng, J. Zhang and L. Zhang, *Chem. – Eur. J.*, 2021, **27**, 16117–16120.
24 D. Wang, Z. N. Chen, Q. R. Ding, C. C. Feng, S. T. Wang, W. Zhuang and L. Zhang, *CCS Chem.*, 2020, **2**, 2607–2616.
25 J. Wang, M. Luo and Q. P. Lin, *J. Solid State Chem.*, 2024, **335**, 124723.
26 H. F. Zhao, W. Z. Chen, S. T. Wang, S. Chen, J. Zhang and L. Zhang, *J. Mater. Chem. C*, 2024, **12**, 4771–4778.
27 M. Mehring, M. Schürmann, K. Jurkschat, H. Reuter and D. Dakternieks, *Angew. Chem., Int. Ed.*, 1997, **109**, 1150–1152.
28 S. Saha, D. H. Park, D. C. Hutchison, M. R. Olsen, L. N. Zakharov, D. Marsh, S. Goberna-Ferron, R. T. Frederick, J. T. Diulus, N. Kenane, G. S. Herman, D. W. Johnson, D. A. Keszler and M. Nyman, *Angew. Chem., Int. Ed.*, 2017, **56**, 10140–10144.
29 X. J. Tian, Y. Z. Yu, Q. Lu and X. M. Zhang, *Inorg. Chem.*, 2022, **61**, 6037–6044.
30 B. Peters, N. Lichtenberger, E. Dornsiepen and S. Dehnen, *Chem. Sci.*, 2020, **11**, 16–26.
31 D. Wang, G. H. Chen, S. T. Wang, J. Zhang and L. Zhang, *Chem. Commun.*, 2022, **58**, 4759–4762.
32 K. Suzuki, T. Hanaya, R. Sato, T. Minato, K. Yamaguchi and N. Mizuno, *Chem. Commun.*, 2016, **52**, 10688–10691.
33 S. Bhattacharya, U. Basu, M. Haouas, P. Su, M. F. Espenship, F. Wang, A. Sole-Daura, D. H. Taffa, M. Wark, J. M. Poblet, J. Laskin, E. Cadot and U. Kortz, *Angew. Chem., Int. Ed.*, 2021, **60**, 3632–3639.
34 C. Zhao, Y. Z. Han, S. Dai, X. Chen, J. Yan, W. Zhang, H. Su, S. Lin, Z. Tang, B. K. Teo and N. Zheng, *Angew. Chem., Int. Ed.*, 2017, **56**, 16252–16256.
35 W. Huang, W. Chen, Q. Bai, Z. Zhang, M. Feng and Z. Zheng, *Angew. Chem., Int. Ed.*, 2022, **61**, e202205385.
36 Q. R. Ding, Y. Yu, C. Cao, J. Zhang and L. Zhang, *Chem. Sci.*, 2022, **13**, 3395–3401.
37 R. D. Lai, J. Zhang, X. X. Li, S. T. Zheng and G. Y. Yang, *J. Am. Chem. Soc.*, 2022, **144**, 19603–19610.
38 S. Bhattacharya, U. Basu, M. Haouas, P. Su, M. F. Espenship, F. Wang, A. Sole-Daura, D. H. Taffa, M. Wark, J. M. Poblet, J. Laskin, E. Cadot and U. Kortz, *Angew. Chem., Int. Ed.*, 2021, **60**, 3632–3639.
39 L. Fan, Z. Xia, M. Xu, Y. Lu and Z. Li, *Adv. Funct. Mater.*, 2018, **28**, 1706289.
40 J. T. Feaster, C. Shi, E. R. Cave, T. Hatsukade, D. N. Abram, K. P. Kuhl, C. Hahn, J. K. Nørskov and T. F. Jaramillo, *ACS Catal.*, 2017, **7**, 4822–4827.
41 D. D. Zhu, J. L. Liu and S. Z. Qiao, *Adv. Mater.*, 2016, **28**, 3423–3452.
42 Y. Deng, J. Zhao, S. Wang, R. Chen, J. Ding, H. J. Tsai, W. J. Zeng, S. F. Hung, W. Xu, J. Wang, F. Jaouen, X. Li, Y. Huang and B. Liu, *J. Am. Chem. Soc.*, 2023, **145**, 7242–7251.
43 R. Samanta, M. Kempasiddaiah, R. K. Trivedi, B. Chakraborty and S. Barman, *ACS Appl. Energy Mater.*, 2024, **7**, 5359–5370.
44 B. Sun, Z. Li, D. Xiao, H. Liu, K. Song, Z. Wang, Y. Liu, Z. Zheng, P. Wang, Y. Dai, B. Huang, A. Thomas and H. Cheng, *Angew. Chem., Int. Ed.*, 2024, **63**, e202318874.
45 Z. Guo, Y. Yu, C. Li, E. Campos dos Santos, T. Wang, H. Li, J. Xu, C. Liu and H. Li, *Angew. Chem., Int. Ed.*, 2024, **63**, e202319913.
46 X. Mei, C. Liu, D. Zhang, J. Cao, R. Ge, J. Wang and W. Xu, *Adv. Energy Mater.*, 2024, **14**, 2303889.